28905 DUP.

IGM88TC-204-725-G
CNRC 28905

THE EFFECT OF SAND CONCENTRATION ON THE EROSION OF MATERIALS BY A SLURRY JET

S. Turenne*, M. Fiset** and J. Masounave*

*Industrial Materials Research Institute
NATIONAL RESEARCH COUNCIL CANADA
75 De Mortagne
Boucherville (Qc) Canada
J4B 6Y4

Laval University
Mining and Metallurgical Dept.
Quebec (Qc) Canada
G1K 7P4

Abstract

Slurry erosion tests were performed in order to evaluate the effect of sand concentration on the erosion rate. By maintaining the slurry velocity constant, different particle fluxes were obtained by varying the sand concentration in the slurry. The erosion tests were done with an erosion machine giving a narrow slurry jet which had a velocity of 17 m/s. The slurry jet was always oriented toward the surface with a normal incidence angle. It was observed that the erosion rate decreased according to a power law of the sand concentration in the slurry. This effect can be attributed to the rebounding particles which protect the surface against incident particles. The amplitude of this effect also depends on the incidence angle of individual sand particles which are forced to deviate near the surface. Because there is a distribution of incidence angle near the surface, the relation between the protection effect and the incidence angle can explain partially the erosion profile of the eroded surface.

Symbols

C: sand mass fraction in the slurry (g/g)

d: jet diameter (m)

f: sand volume fraction in the slurry (cm^3/cm^3)

F: particle flux ($g/cm^2 \cdot s$)

h: erosion depth (mm)

h_{max}: maximum erosion depth (mm)

m_ℓ: liquid mass (g)

m_s: sand mass (g)

M: total mass of abrasive used in a test (g)

t: duration of a test (s)

v: slurry velocity (m/s)

V_ℓ: liquid volume (cm^3)

V_s: sand volume (cm^3)

W: wear value expressed as a mass loss (g)

x: distance from the center of the erosion spot (mm)

α: incidence angle of particle

ρ_ℓ: liquid density (g/cm^3)

ρ_s: sand density (g/cm^3)

1- INTRODUCTION

The effect of particle flux on the dry erosion rate was studied by some authors [1-4]. In most of these studies, it was observed that the erosion rate (g/g) decreased as the particle flux increased. This behavior was associated with the fact that the abrasive particles, after impinging the surface, rebound and protect the exposed surface against the incident abrasive particles. Anand et al. [4] had developed a first-order particle collision model in order to quantify the flux effect. They reported that the erosion rate decreased exponentially as the particle flux increased with an exponent proportional to the average path length of a rebound particle. This path length corresponds to the height of the rebound cloud over the test surface.

When one considers the case of slurry erosion, the particle path should be different because the viscosity of the fluid is high enough to force the particle to follow the streamline near the surface. Especially the large particles, having more inertia than the small ones, resist deviation [5]. The fluid movement therefore deflects the rebounding particles which have a reduced velocity. This results in a lowered height of the rebound cloud. For this reason, the analogy with the model mentioned above is very limited.

The purpose of this study is to quantify the flux effect in the case of slurry erosion by a narrow jet. The variation of the flux effect with the incidence angle, suggested by Anand et al. [4], will be considered to explain the erosion profile at the surface which is known to be related to the incident angle of the particles impinging the surface. The results of slurry erosion obtained by Benchaita et al. [5,6] correspond to a case where the protection brought about by the rebounding particles is negligible because the sand concentration was very low (0.32% wt). However, their evaluation of the particle path in the slurry jet near the surface will be used in the discussion of the influence of the protective rebounding cloud on the erosion profile.

2- EXPERIMENTAL

Erosion tests were done with an erosion apparatus using an air-powered double-diaphragm slurry pump. It is shown schematically in Figure 1. The slurry was pumped from a tank containing a volume of nearly 7 litres of slurry, projected against the surface of the sample at a normal incident angle and returned to the tank. The slurry jet had a diameter of 4.76 mm. The silica sand concentration in the slurry was determined after using the same amount of water (6.4 litres) in each case but a different amount of silica sand. Concentrations of 1, 5, 10, 15 and 20% were employed. For sand concentrations higher than 20%, the slurry pump employed was found inadequate. The size distribution of sand particles lay between 200 and 300 μm. The slurry velocity was measured by an electromagnetic flowmeter. It was kept constant at 17 m/s for all tests. The velocity of the abrasive particles has been assumed approximately equal to the velocity of the slurry jet. This approximation is justified by the high sand concentrations used in our tests which limit the velocity of the fluid relative to the particle velocity.

The sample blocks were made of pure aluminum with dimensions of 2.5 cm x 2.6 cm x 1 cm. One sample of glass was also used for the study of the erosion profile. Before and after the erosion tests, the samples were cleaned in an ultrasonic bath, dried and weighed with a precision of ±0.1 mg. The mass loss of the samples was defined as the wear value. The 20 minutes test duration was chosen in order to obtain significant mass losses.

For the observation of the erosion profile, two samples of aluminum and glass were mounted in epoxy. The mountings were cut perpendicularly to the worn surfaces in the middle of the erosion spot. Micrographs of the profiles were taken by optical microscopy; the erosion depth along the profiles could be measured directly on these micrographs.

3- RESULTS AND DISCUSSION

3.1- Erosion rate vs sand volume fraction

For the different sand mass fractions used, the erosion tests were interrupted every five minutes to observe the evolution of the erosion rate. The mass losses are plotted as a function of testing time in Figure 2. The mass removal is shown to be proportional to the testing time for all sand concentrations. One should not relate directly the slope of the straight lines to the erosion rate because the masses of abrasive used for the 20 minutes test duration are not the same and depend on the sand concentrations. Despite that no measurement was taken for very short test duration, the fact that these regression lines pass through the origin suggests the absence of an incubation period. In the following description of the results, the wear values will correspond to the mass loss of samples after 20 minutes of testing.

For a given test duration, the wear increases with sand concentration because of the higher amount of erodent particles used to impinge the surface of the sample. However the erosion efficiency, which is defined as the ratio of the wear value to sand concentration, decreases as the sand concentration increases. This behavior is illustrated in Figure 3. For concentrations higher than about 13%, the erosion efficiency becomes constant. The decrease of the erosion efficiency is an indication of particle interaction which impedes the erosion of the sample. The laminar flow of the slurry jet becomes turbulent near the surface of the sample and the resulting flow conditions lead to a particle cloud which protects the surface. For concentrations at which the erosion efficiency is nearly constant, the gain in erosion brought about by an increase in the amount of particles is compensated by a gain in the protection effect. For very low concentrations, one can suppose that the small amount of particles in the flow leads to a low density cloud which brings almost no "screening effect".

For the following analysis, it is more convenient to express the

concentration in the form of sand volume fraction instead of sand mass fraction. From the relations expressing the mass fraction C and the volume fraction f:

$$C = \frac{m_s}{m_s + m_\ell} \tag{1}$$

$$f = \frac{V_s}{V_s + V_\ell} \tag{2}$$

where the subscripts s and ℓ refer to sand and liquid respectively, it is straightforward to show that:

$$f = \frac{1}{1 + \frac{\rho_s}{\rho_\ell}\left(\frac{1}{C} - 1\right)} \tag{3}$$

ρ_s and ρ_ℓ correspond to the densities of the sand and the liquid. With a sand density of 2.65 g/cm^3 and water as the liquid phase, the sand volume fraction is illustrated as a function of the mass fraction in Figure 4. Within the range of mass concentration studied, the volume fraction f maybe considered roughly proportional to the mass fraction C.

If we use the approximation that the abrasive particle velocity is the same as the slurry velocity v, the relation for the particle flux F ($g \cdot cm^{-2} \cdot s^{-1}$) is given by:

$$F = v\rho_s f \tag{4}$$

This relation means that only the volume fraction of abrasive particles is considered in the wear processing of the sample surface. By multiplying the particle flux by the cross section of the jet and by the test duration t, the total mass M of abrasive particles which impinged the surface during the test can be determined:

$$M = F \cdot (\pi d^2/4) \cdot t \qquad (5)$$

The erosion rate is defined as the ratio of mass loss to the mass of abrasive used. In Figure 5 the erosion rate W/M is plotted on a log-log scale as a function of the abrasive volume fraction in the slurry. The values were computed by using the following experimental conditions:

$\rho_s = 2.65$ g/cm^3 $\qquad$ $v = 1700$ cm/s
$d = 0.476$ cm $\qquad$ $t = 1200$ s (20 min)

The computed values of the particle fluxes and erosion rates are reported in Table 1. The following empirical relation fits the experimental data with a correlation coefficient of 0.99:

$$\frac{W}{M} = \frac{4.55 \times 10^{-7}}{f^{0.33}} \qquad (6)$$

The results show that, for the concentration range studied, a power law of the volume fraction gives a better fit than the exponential law proposed by Anand et al. [4] in their model for dry erosion. If we consider only the three lower concentrations (1, 5 and 10% wt), which is about within the flux range studied by these authors, the exponential law fits the data with a correlation coefficient of 0.98. The range of particle fluxes in our experiments is approximately three times larger than the one investigated by these authors. As it was mentioned earlier, the flow characteristics near the surface are probably totally different due to the difference in fluid viscosity.

From the analysis of the curves of Figures 3 and 5, it is possible to define a parameter to express the abrasivity of the erodent particles in the slurry. This parameter could be the erosion rate corresponding to a low concentration, of 0.5% for example, where it is known that no protection occurs from the rebounding particles.

TABLE 1

C	f	W (mg)	M (kg)	W/M ($\times 10^{-6}$ g/g)	F ($g/cm^2 \cdot s$)
0.01	0.0038	9.8	3.646	2.69	6.46
0.05	0.0194	32.8	18.700	1.75	32.98
0.10	0.0402	50.4	38.643	1.30	68.34
0.15	0.0623	67.1	59.957	1.12	105.91
0.20	0.0861	87.8	82.789	1.06	146.37

3.2- Erosion profiles

From the micrographs of erosion profiles, the erosion depth h was measured from one edge of the erosion spot to the other. Because of the radial symmetry, the mean of the two erosion depth values at the same distance x from the center was considered. In order to compare the erosion profiles of aluminum and glass, the erosion depth measurements were normalized with respect to the maximum depth value h_{max} along the profiles. The graphics illustrating the profiles for both materials are shown in Figure 6. The general behavior is the same for both materials: the radius of the spot is nearly 6 mm with a maximum erosion depth occurring at approximately 4 mm from the center. Two differences between the profiles of aluminum and glass may however be pointed out: 1) the normalized erosion depth at the center of the spot (x = 0) is higher for glass than for aluminum and 2) the maximum erosion depth takes place for a higher value of x in the case of aluminum.

To interpret the erosion profiles, it is important to know the incidence angle of individual particles all along the eroded surface. It is evident that even if the jet is oriented with a given incidence angle, there is a distribution of incidence angles of particles near the surface of the sample. Benchaita et al. [5] have proposed a model to determine the normal and tangential components of the particle velocity near the surface which depend on the position of the particle in the flow. This model suggests that for a normal incidence of the jet, the particles impinge the surface at 90° in the center of the spot and with a continuously decreasing incidence angle away from the center. Consequently, the tangential component of the particle velocity increases considerably when getting away from the center of the spot. Figure 7 illustrates that the eroded surface looks quite different in the middle and in the deepest part of the erosion spot for the aluminum. In the latter region, the erosion craters produced by single particle impact are elongated in the direction of particle movement compared to those in the center. The low incidence angle and the high tangential velocity of the particle can explain the higher efficiency of the microcutting mechanism in the region of maximum erosion.

As shown in Figure 6, the normalized erosion at the center of the spot (i.e. $x = 0$) for glass is higher than for aluminum. The maximum erosion for aluminum takes place at a higher distance from the center (i.e. lower incidence angle) than for glass. This is in good agreement with the behavior of ductile materials. Nevertheless, the distribution of the incidence angle of particles near the surface cannot explain entirely the erosion profiles. For the erosion profile of glass, the maximum erosion occurs at an incidence angle of particles of less than 90° whereas the well known characteristic of a brittle material predicts maximum erosion at 90°.

The effect of local incidence angle on the screen effect can partially explain the occurrence of maximum erosion at intermediate incidence angles for ductile and brittle materials. The thickness of the rebounding cloud depends on the incidence angle. The first-order model of Anand et al. [4] proposes a linear relation between the erosion rate and the factor sin 2α:

$$\ln (W/M) \propto - (p_1 - p_2 \sin 2\alpha) \qquad (7)$$

where p_1 and p_2 are two functions of testing parameters. It can be easily deduced geometrically that the factor sin 2α is inversely proportional to the thickness of the cloud measured along the direction of the incident jet. From this model, the value of sin 2α is maximum for an incidence angle α of 45°. This means that for this incidence angle near the surface, the thickness of the rebounding cloud is minimized and the erosion process is more efficient. From the micrographs of the eroded surface in the maximum erosion region (Fig. 7), the shape of the craters suggests an intermediate incidence angle between 0° and 90°. Even if the model for dry erosion does not apply in the present case, it is plausible that the cloud protection effect is minimal for an incidence angle smaller than 90°. The screening effect does not depend on the material tested; for this reason, the erosion profiles for aluminum and glass are similar.

Our experiment does not permit to evaluate the magnitude of the screening effect but it is surely not the only factor leading to the erosion profiles

observed. The particle velocity is also a preponderant parameter which influences the erosion profile. The higher tangential velocity encountered out of the center of the erosion spot favours the microcutting process associated with high wear rates of ductile materials. It is well known that the erosion rate is proportional to the particle velocity to the power n. With our experimental apparatus, n is nearly equal to 4 [7]. Then a small increase in particle velocity results in an important augmentation of the erosion rate.

From the arguments mentioned about the distribution of incidence angle and particle velocity, the true influence of the incidence angle on the erosion rate cannot be obtained. The modification of incidence angle and particle velocity should be less important for dry erosion and in the case where large abrasive particles are employed. With the knowledge of incidence angle and particle velocity for each point of the eroded surface, it is possible to deduce the wear versus incidence angle characteristic from the analysis of the profile obtained from a single erosion test with normal incidence angle of the slurry jet.

4- SUMMARY

This study on the effect of sand concentration emphasizes the following features:

- The erosion rate decreases according to a power law of the sand volume fraction with an exponent of about 1/3.

- The screen effect at the surface of sample is dependent on the incidence angle of the particles.

- The slurry erosion test done with the apparatus described produces an erosion profile which depends more on the flow behavior of abrasive particles than on the material itself.

ACKNOWLEDGEMENTS

The authors are indebted to G. Huard and J.H. Prinsen for helpful discussions and careful reading of the manuscript.

5- REFERENCES

1- Uuemois, U. and Kleis, I., Wear, 31 (1975) 359.

2- Tilly, G.P. and Sage, W., Wear, 16 (1970) 447.

3- Neilson, J.H. and Gilchrist, A., Wear, 11 (1968) 123.

4- Anand, K., Hovis, S.K., Conrad, H. and Scattergood, R.O., Wear, 118 (1987) 243.

5- Benchaita, M.T., Griffith, P. and Rabinowicz, E., J. Eng. Ind., 105 (1983) 215.

6- Benchaita, M.T., Tribol. Trans., 31 (1988) 133.

7- Turenne, S., Le Dëoré, C. and Masounave, J., to be presented at the "World Materials Congress 1988", Chicago, 26-30 Sept. 1988.

FIGURE CAPTIONS

Fig. 1 Experimental apparatus used for slurry erosion tests.

Fig. 2 Erosion wear W of aluminum as a function of test duration t for different sand mass concentrations.

Fig. 3 Erosion efficiency (W/C) versus sand mass concentration C for the aluminum eroded during 20 minutes.

Fig. 4 The analytical relation between the sand volume fraction f and the mass fraction C is almost linear within the concentration range studied.

Fig. 5 Empirical relation between the erosion rate (W/M) and the sand volume fraction (f) for the aluminum eroded during 20 minutes. The straight line was determined by linear regression.

Fig. 6 The normalized erosion depth $(h(x)/h_{max})$ as a function of the distance x from the center of the erosion spot a) for the aluminum and b) for the glass eroded during 20 minutes by a slurry having a sand mass fraction of 0.10.

Fig. 7 Scanning electron microscope observation of eroded surfaces of aluminum and glass. The regions 1, 2 and 3 correspond respectively to the center, the maximum erosion region and the peripheral limit of the erosion spot. The arrows indicate the direction of erodent particles displacement for the regions 2 and 3.

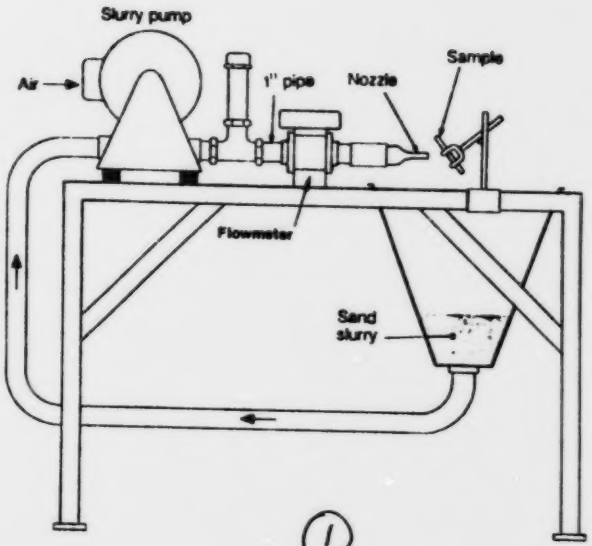
Slurry pump
Air
1" pipe
Nozzle
Sample
Flowmeter
Sand slurry

(1)

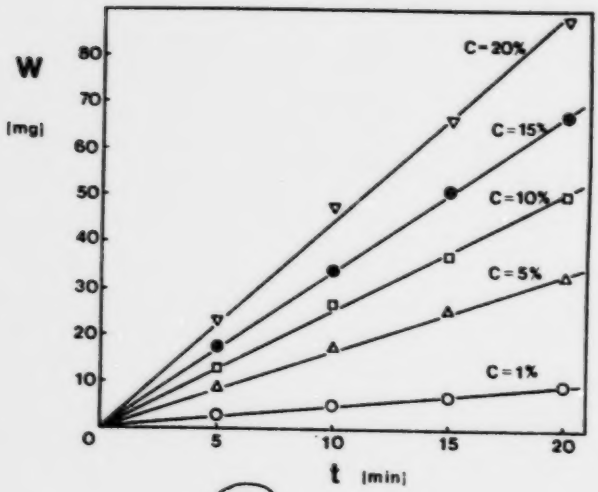
W
[mg]
C=20%
C=15%
C=10%
C=5%
C=1%
t [min]

(2)

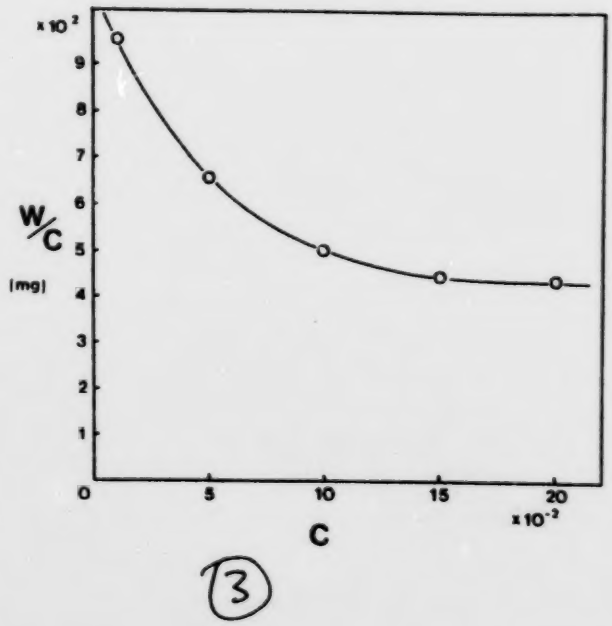
W/C
[mg]
C
x10⁻²

(3)

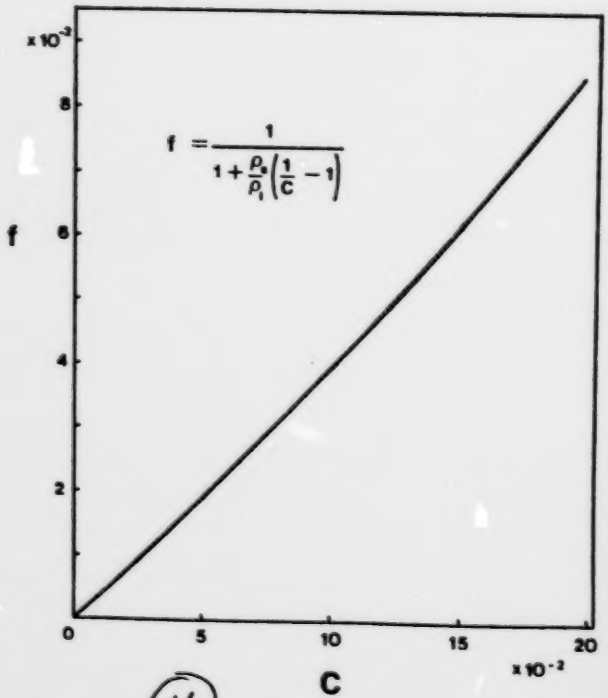
f = 1 / (1 + ρs/ρl (1/C − 1))
f
C
x10⁻²

(4)

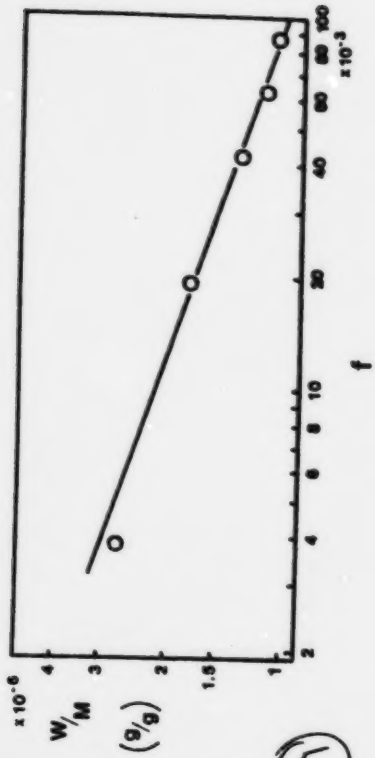

(5)

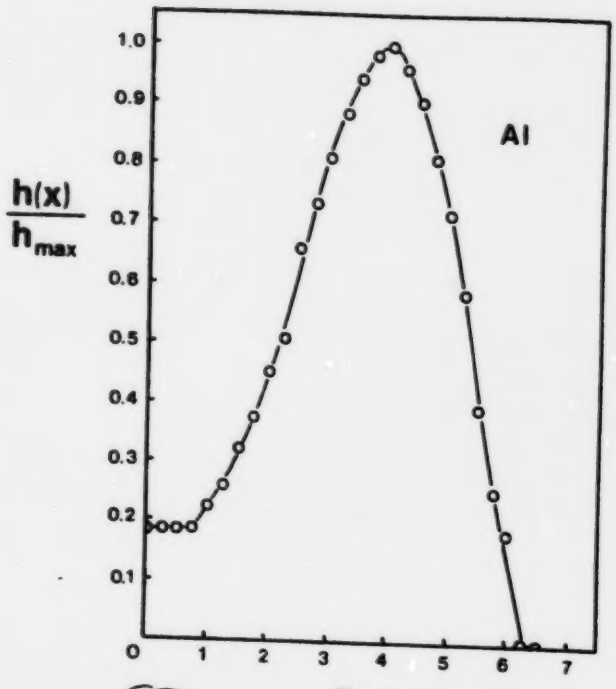

(6a)

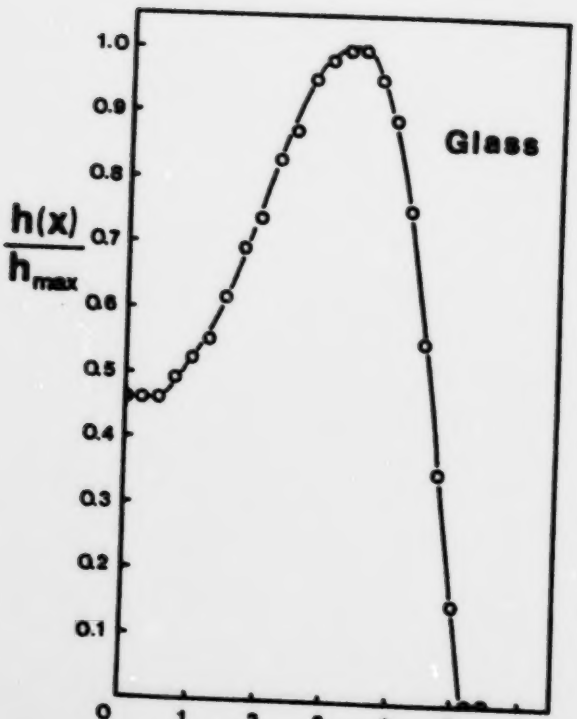

(6b)

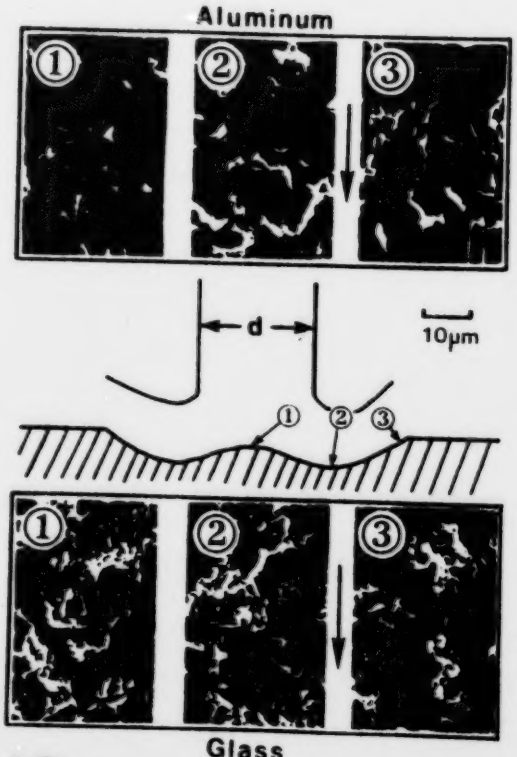

(7)